Investigation of Glutaric Anhydride as an Electrolyte Additive for Graphite/LiNi$_{0.5}$Mn$_{0.3}$Co$_{0.2}$O$_2$ Full Cells

Cameron Peebles,[a] Meinan He,[a,b] Zhenxing Feng,[c] Chi-Cheung Su,[a,d] Li Zeng,[e]
Michael J. Bedzyk,[e,f,g] Paul Fenter,[a,d] Yan Wang,[b] Zhengcheng Zhang,[a] and Chen Liao[a,d,z]

[a]*Chemical Science and Engineering Division, Argonne National Laboratory, Argonne, Illinois 60439, USA*
[b]*Mechanical Engineering, Worcester Polytechnic Institute, Worcester, Massachusetts 01609, USA*
[c]*School of Chemical, Biological, and Environmental Engineering, Oregon State University, Corvallis, Oregon 97331, USA*
[d]*Joint Center for Energy Storage Research (JCESR), Argonne National Laboratory, Argonne, Illinois 60439, USA*
[e]*Applied Physics Program, Northwestern University, Evanston, Illinois 60208, USA*
[f]*Department of Materials Science and Engineering, Northwestern University, Evanston, Illinois 60208, USA*
[g]*Department of Physics and Astronomy, Northwestern University, Evanston, Illinois 60208, USA*

The effects of glutaric anhydride (GA) as an electrolyte additive for graphite/LiNi$_{0.5}$Mn$_{0.3}$Co$_{0.2}$O$_2$ full cells operating between 3.0–4.4 V were investigated. Linear scan voltammetry (LSV) revealed that GA preferentially oxidized prior to the carbonate-based electrolyte while Li/graphite half cells revealed that GA can suppress electrolyte decomposition on the graphite electrode giving rise to the bifunctional nature of this additive. The addition of both 0.5 and 1.0 wt% of GA into the carbonate-based electrolyte resulted in superior cycling performance compared to the baseline electrolyte as demonstrated by the slight increase in initial capacities and significant increases in capacity retention over 117 cycles at C/3. Electrochemical impedance spectroscopy (EIS) showed that while the overall impedance of the GA containing cells was higher than the cells with the baseline electrolyte the change in impedance between post-formation and post-cycling was smallest for the cells containing GA. Additionally, X-ray photoelectron spectroscopy (XPS) analysis confirmed that GA decomposed on the cathode surface leading to an increase in oxygen-containing species, a decrease in LiF species and a simultaneous increase in Li$_x$PO$_y$F$_z$ species.
© 2016 The Electrochemical Society. [DOI: 10.1149/2.0721702jes] All rights reserved.

Lithium ion batteries (LIBs) have demonstrated excellent promise and are the top candidates for powering electric vehicles (EVs) and plug-in hybrid electric vehicles (PHEVs). To obtain the necessary high energy and power densities over numerous charge and discharge cycles that these automobiles will require, new cathode materials are continuously being investigated. Compared to tradition LiMnO$_2$ and LiCoO$_2$ cathode materials, Ni-based layered LiNi$_x$Mn$_y$Co$_z$O$_2$ (NMC, where x + y + z = 1) materials have attracted much attention due to their high capacity, low cost and attractive electrochemical performance.[1–4] While Ni-rich NMC materials display higher capacities at the expense of lower safety (lower thermal stability), Co- and Mn-rich materials show higher safety characteristics but lower capacities.[3] Although these cathode materials are attractive from a high capacity standpoint, the required charge voltages (>4.4 V vs. Li/Li$^+$) to attain this high capacity results in several inherent issues leading to poor electrochemical performance.[5,3,6] Explanations for the observed poor performance of these materials at high voltages include 1) structural changes from layered to spinel upon cycling,[1] 2) Mn- and Ni-dissolution giving rise to surface side reactions at the graphite anode[5] and 3) oxidative instability of conventional carbonate-based electrolytes beyond 4.4 V (vs Li/Li$^+$).[6–8] Numerous strategies have been adapted to overcome continual electrolyte decomposition at the cathode under high voltage operating conditions. Protection of the cathode surface using inorganic oxide coatings (SiO$_2$, Al$_2$O$_3$, TiO$_2$, etc.)[9] and organic polymer coatings (PEDOT)[10] have been successful but require a cathode pretreatment. Additionally, the use of intrinsically stable high voltage electrolyte solutions[11,12] as well as electrolyte additives for electrode-electrolyte interphase stabilization[13–17] have been well explored. Of the previously mentioned strategies, electrolyte additives provide a more economical approach to preventing electrolyte oxidative decomposition. While many additives are able to form a solid-electrolyte interphase (SEI) on carbon-based anodes (such as graphite), relatively fewer additives display the ability to form a protective film on the surface of the cathode. This issue will become more prevalent as high voltage cathode materials emerge necessitating solvents with higher electrochemical stabilities.

Anhydrides have found recent success as electrolyte additives for both passivation on carbonaceous anodes and high voltage cathodes.

The use of glutaric anhydride (GA) was shown to increase the formation of a homogenous fluorophosphates-containing interphase and subsequently lower the formation of LiF (a highly resistive species) when used as an additive for LiNi$_{0.4}$Mn$_{1.6}$O$_4$ (LNMO) surfaces.[18] In another study, Li/LNMO half cells containing succinic anhydride (SA) were cycled up to a cutoff voltage of 4.95 V and displayed reduced capacity loss, the formation of a thinner, more stable SEI, and an improved Coulombic efficiency.[19] During cycling at high voltage (~4.9 V) for Li/LiNi$_{0.5}$Mn$_{1.5}$O$_4$ half cells, SA (3 wt%) used as an additive resulted in the formation of a compact, stable layer on the surface of the LNMO cathode improving the interphase stability at high voltages.[20] Recent work by Guyomard et al.[21] showed an improvement in Li$_4$Ti$_5$O$_{12}$/LNMO full cell cycling performance between 1.5–3.5 V (equivalent to 3.05–5.05 V vs Li/Li$^+$) when GA (2 wt%) was used as an additive. Using XPS analysis they explored the impact of GA on the electrode/electrolyte interface and found that GA forms a passivation film mainly composed of organic compounds (mainly O=C-O containing species) on the LNMO surface.

On the negative anode, additives are crucial in formation of an SEI capable of reducing electrolyte decomposition during the cell cycling. Lithium bis(oxalato)borate (LiBOB) and lithium difluoro(oxalato)borate (LiDFOB) have found continued success as SEI-forming additives due to their high ionic conductivity and their ability to form protective SEI layers on the graphite surface. The previously mentioned SA has also been shown to form a stable SEI on graphite anodes during the first graphite intercalation process.[22] Additives that are capable of passivating the negative electrode while forming a beneficial protective layer on the cathode surface are uncommon but of great interest. Bifunctional additives such as these reduce the need for binary additive solutions and thus reduce the complexity of the electrolyte mixture.

In this work we demonstrate that glutaric anhydride (GA) can be effectively used as an electrolyte additive (in as little as 0.5 wt%) in graphite/NMC532 full cells operating between 3.0–4.4 V. The NMC532 composition was selected as it displays a good balance between thermal stability and high capacity. The additive was shown to suppress electrolyte decomposition on the graphite negative electrode and also displayed a propensity to be oxidized prior to the baseline electrolyte on the NMC positive cathode. After 117 cycles the capacity retention for cells containing GA was higher than for the baseline

[z]E-mail: liaoc@anl.gov

Table I. Composition of cell components.

Positive Electrode	Negative Electrode
90 wt% NMC532 (Toda)	91.8 wt% A12 graphite (Phillips 66 CPreme)
5 wt% PVDF binder (Solvay 5130)	6 wt% PVDF binder (Kureha 9300)
5 wt% C45 (Timcal)	2 wt% C45 (Timcal)
9.17 mg/cm^2 active-maetiral loading density	0.17 wt% Oxalic Acid
34 uM thick coating	5.88 mg/cm^2 active-maeitral loading density
20 uM Al current collector	44 uM thick coating
33.5% porosity	10 uM Cu current collector
	38.4% porosity
Electrolyte	Separator
1.2 M LiPF$_6$ in EC/EMC (3:7 w/w) with 1.0 or 0.5 wt% Glutaric Anhydride (Sigma Aldrich, 95% purity)	25 uM thick (Celgard 2325, PP/PE/PP)

electrolyte and XPS analysis of the NMC cathode surface suggests a more stable and compact surface film is formed in the presence of GA.

Experimental

All electrodes in this study are from Argonne's Cell Analysis, Modeling and Prototyping (CAMP) facility and Table I lists the composition of the electrodes used in this study. The positive electrode material was composed of 90.0 wt% Li$_{1.03}$(Ni$_{0.5}$Mn$_{0.3}$Co$_{0.2}$)$_{0.97}$O$_2$ (Toda), 5.0 wt% PVdF binder (Solvay, 5130) and 5.0 wt% C45 carbon black (Timcal) coated on an aluminum current collector. The loading density of the positive electrode active material was 9.17 mg/cm^2. The negative electrode was composed of 91.8 wt% ConocoPhillips A12 graphite, 6.0 wt% PVdF binder (Kureha, 9300), 2.0 wt% C45 carbon black (Timcal) and 0.17 wt% oxalic acid coated on a copper current collector. The loading density of the negative electrode was 5.88 mg/cm^2. The separator used in the coin cell assembly was Celgard 2325 (PP/PE/PP) and the "baseline" electrolyte used was composed of 1.2 M LiPF$_6$ in EC/EMC (3:7 w/w) (Tomiyama Chemical Industry, Japan). Glutaric anhydride (shown in Figure 1) was purchased from Sigma Aldrich (used as received) and used as an electrolyte additive in 1.0 wt% (88 mM) and 0.5 wt% (44 mM) in the baseline electrolyte.

All electrochemical data were collected using 2032-type coin cell assemblies (with 14, 15 and 16 mm in diameter for positive electrode, negative electrode and separators, respectively) on graphite/NMC532 full cells. Galvanostatic charge/discharge cycling was conducted between 3.0–4.4 V using the following protocol: three initial "formation" cycles at C/10 rate were followed by 117 cycles at C/3 rate with a three hour hold at 4.4 V in between charge/discharge cycles. The electrochemistry data shown is the average of two or three individually cycled coin cells. Capacity and voltage profiles were recorded using a MACCOR electrochemical analyzer. Impedance data (collected after formation cycles and after aging cycles) were collected using a Solartron analyzer operated between 0.01 Hz and 1 MHz with an amplitude of 10 mV. Linear sweep voltammetry was performed using a Bio-Logic VMP3 station in a three-electrode, Swagelok-type cell with Pt as the working electrode and Li metal as both counter and reference electrodes at a scan rate of 10 mV/s. The diameters of the working, counter and reference electrodes were all 8 mm. All electrochemical measurements were performed at 27°C.
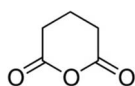
Figure 1. Structure of glutaric anhydride (GA).

To investigate the surface composition of the cycled electrodes and electrolyte the cells were disassembled in an Argon glove box after cycling. The electrodes and separator were first rinsed in CDCl$_3$ (Sigma Aldrich, 99.96 atom %, anhydrous) to study the cycled electrolyte and then rinsed with DMC (Sigma Aldrich, >99%, anhydrous) twice and dried overnight in an inert atmosphere. Scanning electron microscopy (SEM) using a Hitachi S-4700-II microscope in the Electron Microscopy Center of Argonne National Laboratory was employed to observe changes to the bulk morphology of the electrodes before and after cycling. X-ray photoelectron spectroscopy (XPS) spectra were collected at the Keck II facility of NUANCE at Northwestern University with Thermo Scientific ESCALAB 250Xi using monochromated Al Kα X-Rays. A low-energy electron flood gun was used to compensate the XPS-induced surface charging effects. The C1s peak at 284.8 eV was used as the reference to calibrate the XPS spectra. Nuclear magnetic resonance (NMR) of the CDCl$_3$ rinsing solutions were obtained using a Bruker Avance III HD 300 MHz spectrometer. ^{1}H NMR spectra were taken and the chemical shifts are given in parts per million (ppm) relative to a tetramethylsilane standard.

Results and Discussion

Linear scan voltammetry and Li/graphite half cell measurements.—To investigate the anodic stability of GA, linear sweep voltammetry was performed on a Pt working electrode at a scan rate of 10 mV/s at room temperature. The baseline electrolyte displays an increase in oxidation current at ∼6.3 V (vs Li/Li$^+$) indicating substantial electrolyte decomposition (Figure S1 in the Supporting Information shows the baseline electrolyte oxidation peak using a different scale). When 1.0 wt% of GA was added to the solution the oxidation current initially increased between 4.0–6.0 V at which point it drastically increased beyond ∼6.0 V. These results demonstrate that GA preferentially oxidizes prior to the baseline electrolyte on the cathode and may possibly suppress electrolyte oxidation reactions at the cathode-electrolyte interphase.

Interestingly, the cathodic stability of GA is less than that of the baseline electrolyte and shows a reduction peak maximum at ∼2.2 V (vs Li/Li$^+$) as shown in Figure 2b. On the contrary, the baseline electrolyte shows a sharp decrease in reduction current at ∼0.5 V indicative of electrolyte decomposition. The differential capacity plots of first graphite-lithiation cycle for Li/graphite cells containing the baseline electrolyte with and without 1.0 wt% GA are shown in Figure 2c. During the first lithiation the baseline electrolyte shows a peak beginning at ∼0.7 V (vs. Li/Li$^+$) (electrolyte reduction) while the cell containing GA shows a peak beginning at ∼1.1 V. The discrepancy between the reduction potential of GA in Figures 2b and 2c originates from the different working electrodes: in Figure 2b, Pt was used as the working electrode and the measurement was carried out in a beaker cell; while in Figure 2c, graphite was used as the working electrode and the measurement was carried out in a Li/graphite half cell. Neither of these peaks were observed during the second lithiation cycle and therefore are associated with the initial formation of the SEI on the graphite anode. The absence of the lower voltage (∼0.7 V) peak for the cell containing GA (in Figure 2c) indicates that GA can suppress electrolyte reduction on the graphite anode and act as a graphite passivating agent. These results are corroborated by looking at the 1st charge cycle differential capacity plots for graphite/NMC532 full cells with and without GA in the electrolyte (Figure 2d). The baseline electrolyte shows a peak maximum at 3.2 V corresponds to electrolyte reduction on the graphite anode. The cell containing GA shows two stronger peaks at 1.9 and 2.75 V and a small shoulder peak at 3.2 V further suggesting that GA can suppress reduction of the electrolyte on the graphite anode. This is further corroborated by Figure S2 in the Supporting Information which shows that GA can suppress PC solvent co-intercalation into graphite. Put together, the LSV and Li/graphite half-cell results demonstrate that GA is able to both preferentially oxidize prior to the baseline electrolyte on the cathode electrode and also passivate the graphite anode and suppress electrolyte reduction.
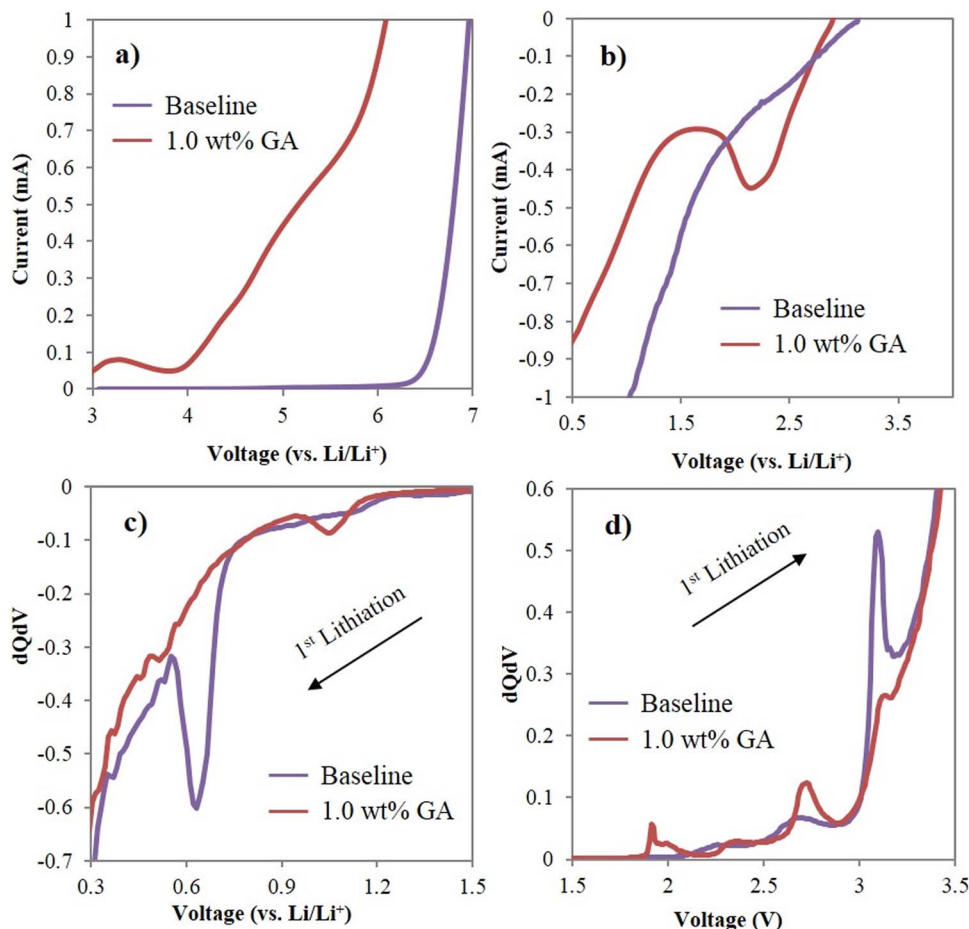
Figure 2. Linear sweep voltammetry of baseline electrolyte with and without 1.0 wt% GA showing (a) anodic stability and (b) cathodic stability; (c) differential capacity plot of Li/graphite half-cell at a C/10 rate; (d) differential capacity plot of graphite/NMC532 full cells showing 1st charge cycle.

Electrochemical cycling and impedance measurements.—Figure 3 shows the cycling performance, Coulombic efficiency and voltage profiles of graphite/NMC532 full cells with and without GA as an additive operating between 3.0–4.4 V. The presence of GA as additive in either 1.0 or 0.5 wt% significantly improved the cycling stability of full cells. For the baseline electrolyte without GA the initial charge and discharge capacities are 221.8 and 192.4 mAh/g, respectively, which correspond to a Coulombic efficiency of 86.8%. For the cells containing 1.0 and 0.5 wt% GA the initial charge and discharge capacities are 223.7 and 195.6 and 222.3 and 194.2 mAh/g, respectively. The resulting first cycle Coulombic efficiencies for 1.0 and 0.5 wt% GA both are 87.4%, slightly higher than the baseline electrolyte. After 117 cycles at C/3 rate, the discharge capacities and Coulombic efficiencies for the baseline electrolyte, 1.0 and 0.5 wt% GA are 167.4 mAh/g and 99.82%, 178.0 mAh/g and 99.89% and 177.7 mAh/g and 99.86%, respectively. These final discharge capacities correspond to capacity retentions of 90.3, 94.8 and 95.2 for the baseline electrolyte, 1.0 and 0.5 wt% GA containing cells, respectively.

Electrochemical impedance spectroscopy (EIS) of the graphite/NMC full cells with and without GA as an additive was conducted to investigate the interfacial impedance of the cathode surface layer. The impedance was measured at a ∼50% state of charge (3.75 V). Three features are evident in the EIS spectra: 1) a high-frequency arc arising from Li$^+$ migration through the SEI film at the positive electrode (R_{SEI}), 2) a mid-frequency arc arising from contributions from both electrodes and associated with charge transport across electrode-electrolyte interface (R_{CT}) and 3) a Warburg tail arising from bulk Li$^+$ diffusion in the electrolyte and the solid phase of electrodes (W_C).[6,13] The initial impedance is denoted

as $R_{initial}$. Figure 4 presents the EIS data for the cells after three C/10 formation cycles and then after 117 charge-discharge cycles at a C/3 rate. Values for the impedance data are in Table II. EIS resistances were estimated by fitting the impedance spectra using the equivalent circuits shown in the figure. Before cycling the high-frequency arc for all cells are similar while the mid-frequency arc decreases in the order 1.0 wt% GA > 0.5 wt% GA > baseline electrolyte. This indicates that increasing the amount of GA in the cell increases the charge transfer resistances at the cathode electrode-electrolyte interface at least after formation cycling. In other words, the oxidized species of GA formed on the surface of the cathode may be composed of more resistive layers compared to the oxidized electrolyte species.

After cycling at a C/3 rate for 117 cycles the mid-frequency charge-transfer resistances of all the cells increased in the order 1.0 wt% GA > 0.5 wt% GA > baseline electrolyte. The initial SEI and the high-frequency arc increased for all cells as well. The overall difference in the R_{CT} (ΔR_{CT}) and R_{SEI} (ΔR_{SEI}) after-formation and after-cycling showed the same trends with the change in the 1.0 wt% GA being the smallest followed by 0.5 wt% GA with the greatest difference occurring in the baseline cell. The change in ΔR_{CT} and ΔR_{SEI} help indicate the extent of resistive surface film formed between the initial "formation" cycles and the final aging cycles. Interestingly, although the initial R_{CT} increased with an increasing wt% of GA the ΔR_{CT} increased the least for the cells containing GA. This suggests that the surface film formed during the initial "formation" cycles plays a role in the subsequent surface film buildup during the aging cycles. Said another way, increasing the wt% of GA in the cell decreased the overall impedance of the surface film formed after the initial "formation" cycles although the overall impedance was greater after 120 cycles. This
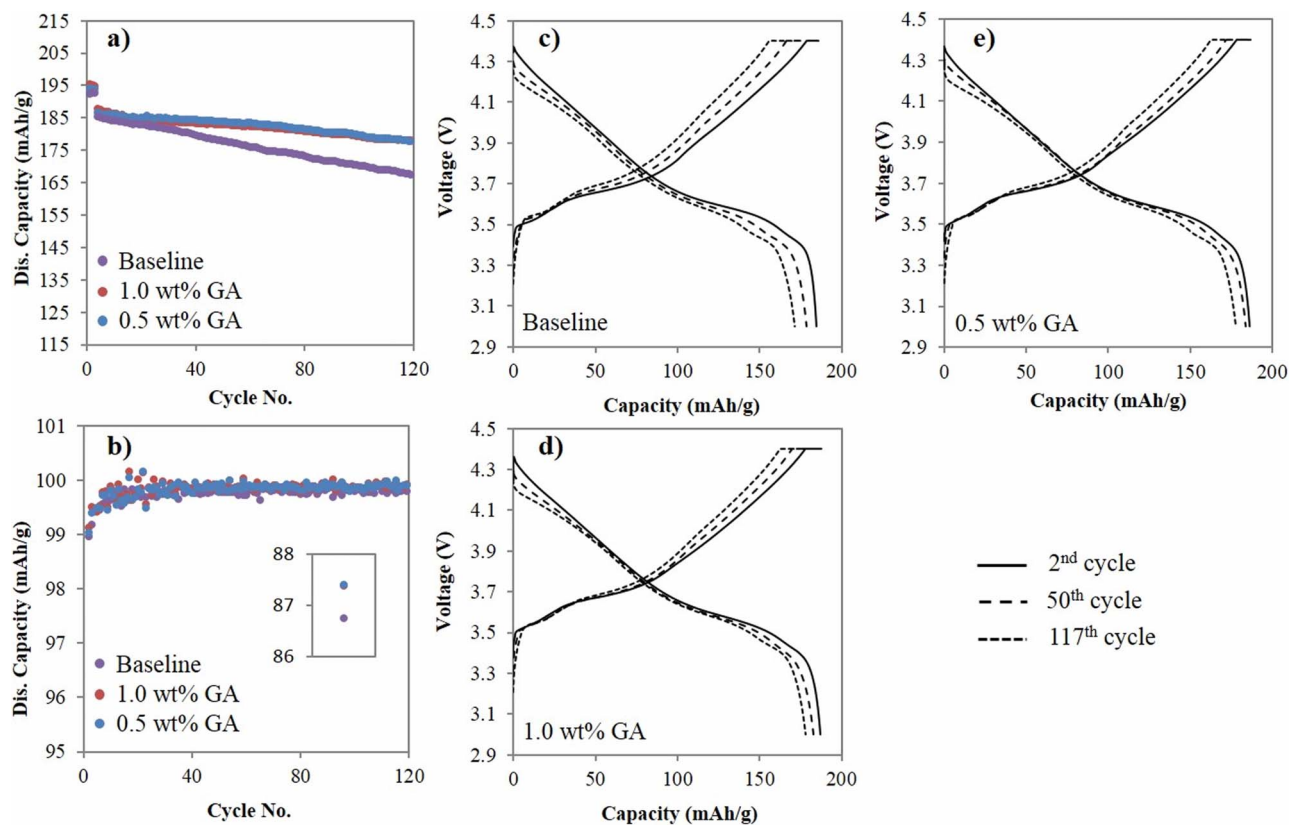
Figure 3. a) Cycling performance, b) Coulombic efficiency, and c)-e) voltage profiles of graphite/NMC532 full cells without (baseline electrolyte) and with 1.0 and 0.5 wt% GA as an electrolyte additive. The inset of b) shows the CE for the 1st cycle.
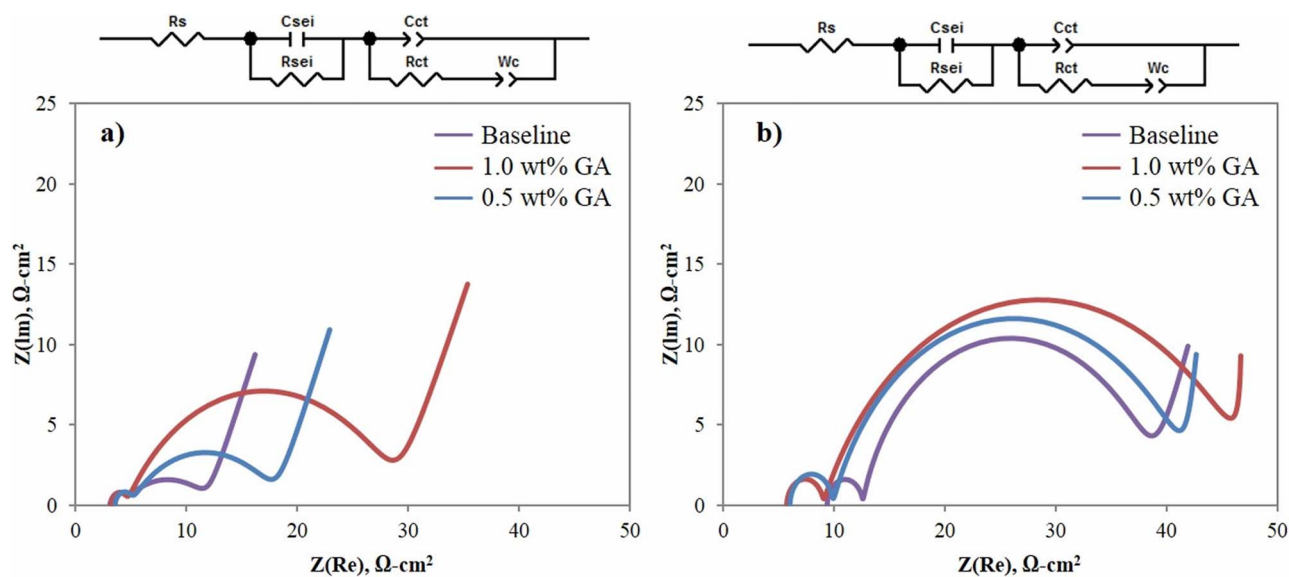
Figure 4. Electrochemical impedance spectroscopy showing the change in impedance after a) formation cycles and b) 117 cycles between 3.0–4.4 V fitted using the equivalent circuits shown. The data was acquired at 3.75 V.

Table II. $R_{Initial}$, R_{SEI} and R_{CT} values for the measured EIS plots.

Cell	After 3rd C/10 formation cycle			After 117th C/3 cycle			Difference in EIS		
	$R_{Initial}$	R_{SEI}	R_{CT}	$R_{Initial}$	R_{SEI}	R_{CT}	$\Delta R_{Initial}$	ΔR_{SEI}	ΔR_{CT}
Baseline	3.1	4.4	11.1	9.3	12.7	38.8	6.2	8.3	27.7
1.0 wt% GA	3.2	4.7	28.6	5.7	9.1	45.9	2.5	4.4	17.3
0.5 wt% GA	3.6	5.0	17.7	5.9	11.1	41.0	2.3	6.1	23.3
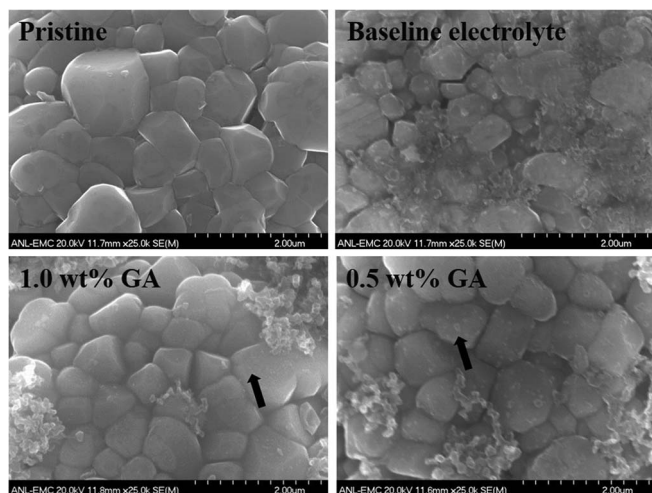
Figure 5. SEM images of a pristine NMC electrode and NMC electrodes cycled with and without GA as an electrolyte additive.

Table III. Elemental composition of the C 1s, O 1s, F 1s and P 2p energies studied.

	C 1s (%)	F 1s (%)	O 1s (%)	P 2p (%)
1.0 wt% GA	64.02	10.82	23.29	1.88
0.5 wt% GA	61.55	19.12	17.67	1.65
Baseline	62.11	25.80	10.64	1.45
Pristine	66.26	29.07	4.67	—

behavior is consistent with other studies which show that although there is an initial increase in impedance with an additive, later cycles may show a net reduction in impedance growth.[23] Impedance data derived from reassembled cells (Supporting Information, Figure S3) indicates that the impedance contribution from the positive electrode is substantially greater than impedance from the negative electrode. This observation has been previously reported in other work where the main contributor to impedance growth in graphite /layered oxide -based full cells is due to changes at the cathode electrode-electrolyte interface.[6] Put together, the impedance data from the cycled cells indicates that a more resistive surface film is formed on the cathode surfaces in cells containing GA even though better cycling performance is observed.

Electrode surface morphology and composition.—Representative SEM images of the $LiNi_{0.5}Mn_{0.3}Co_{0.2}O_2$ electrodes in the pristine state, and cycled state with and without GA as an additive are shown in Figure 5. In the pristine electrode primary particles have a smooth surface and no dark patches or spots are observed. The electrode cycled in the baseline electrolyte without any GA show darker patches on some primary particles indicative of electrolyte decomposition (the rope-like material is C45 carbon black). With the exception of the C45 carbon black, the only observable surface features on the electrodes cycled with 0.5 or 1.0 wt% GA are small island-like deposits (which are yet smaller for the 1.0 wt% GA cells). Images of the cycled baseline electrolyte graphite negative electrode (Supporting Information, Figure S4) look very similar to the cycled negative electrodes of the cells containing 1.0 and 0.5 wt% GA. Whereas the pristine graphite anode has sharp edges and more flaky surfaces, the cycled electrodes display rounder edges and less flaky surfaces indicative of electrolyte decomposition species.

XPS analysis was conducted to gain a more thorough understanding of the surface composition of pristine and cycled $LiNi_{0.5}Mn_{0.3}Co_{0.2}O_2$ electrodes and the results are given in Figure 6. Prior to analysis, the cycled electrodes were rinsed with $CDCl_3$ and DMC to remove residual electrolyte and then allowed to dry. The elemental concentrations of the pristine and cycled electrodes are given in Table III. Any changes made to the top ∼2–5 nm on the surface of the cathodes due to cycling and electrolyte/additive degradation should be noticed.[13] The C 1s carbon amorphous peak at 284.8 eV was used as the reference to calibrate the XPS spectra.

The pristine cathode surface is mainly comprised of species related to the PVdF binder and conductive carbons. The C 1s spectrum shows multiple peaks at 290.5 ($-CF_2-$ in binder and possible Li_2CO_3),[24] 286.3 ($-CH_2-$ in binder) and a large peak at 284.8 eV (C-C, C-H from carbon black and other amorphous carbons).[25] An additional peak at
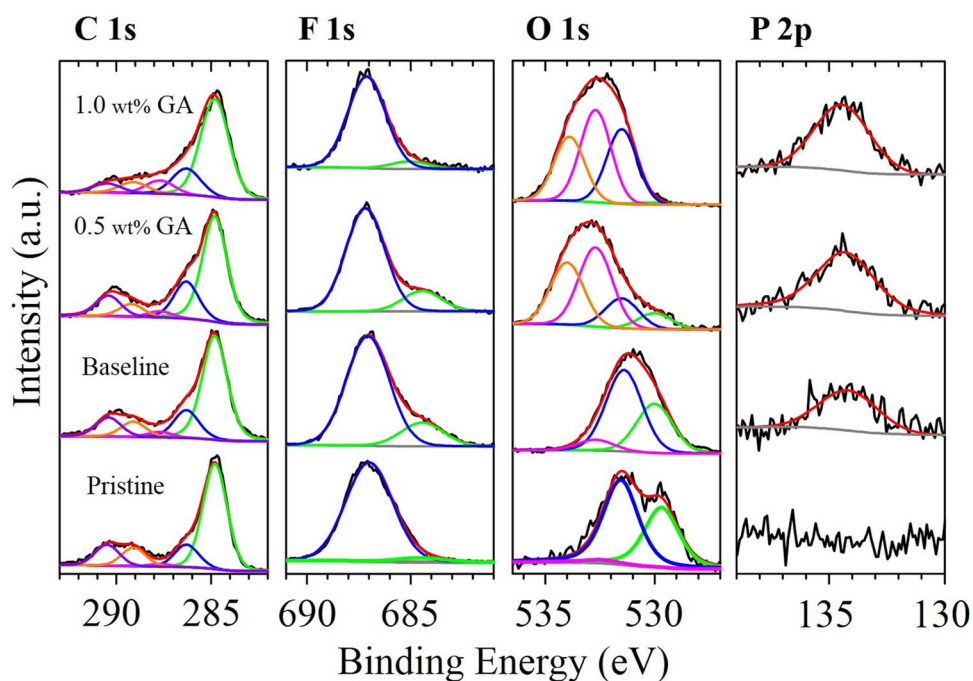
Figure 6. XPS spectra of pristine cathode electrodes and those cycled with and without GA as an electrolyte additive.

289.0 eV may represent O-C=O containing surface species.[6,20,21] The F 1s spectrum is composed of one peak at 687.0 eV (-CF$_2$- in binder).[24] The O 1s spectrum shows two peaks at 531.5 (corresponding to low coordination oxygen atoms[7] and possible Li$_2$CO$_3$[26] and 529.6 eV (LiNi$_{0.5}$Mn$_{0.3}$Co$_{0.2}$O$_2$ metal-O bond).[14] No peaks are present in the P 2p spectrum.

After cycling the surface composition of all cells is drastically different. For the baseline cell containing no additive the C 1s spectrum the intensity of the peak attributed to C-O species at 286.3 eV[14] grew relative to the PVdF binder peak at 290.5 eV. In the F 1s spectrum a new peak at 684.5 eV appeared corresponding to LiF, a common LiPF$_6$ decomposition species.[21] The metal-O bond in the O 1s spectrum decreased in intensity relative to the peak at 531.5 eV and a new peak appeared at 533.0 eV indicative of more oxygen-containing species on the cathode surface. In the P 2p spectrum a new peak at 134.5 eV appeared corresponding to Li$_X$PO$_Y$F$_Z$ species.[27] The F1s peak for Li$_X$PO$_Y$F$_Z$ overlaps with the PVdF binder at 687.0 eV. The decreased peak intensities from the binder, the conductive carbon and the metal-O bond together with an increase in LiF, alkyl carbonates and Li$_X$PO$_Y$F$_Z$ species signifies a different cathode surface film composed of decomposed electrolyte.

For the cycled cells containing GA as an additive some clear trends to the cathode surface species are present. In the C 1s spectrum the amorphous carbon peak at 284.8 eV broadens for both 1.0 and 0.5 wt% GA containing cells suggesting an enhanced deposition of alkyl-containing species. The peak at 286.3 eV (corresponding to C-O species) increases relative to the -CF$_2$- binder peak at 290.5 eV for both 1.0 and 0.5 wt% GA with the higher wt% GA seeing a larger peak increase. For the cell containing 1.0 wt% GA a new peak at 287.5 eV appears which likely corresponds to C=O species[21] and a subsequent increase in the peak at 289.0 eV (O-C=O species) occurs. As indicated in Figure 6, increasing the wt% of GA in the cell leads to a decrease in the amount of LiF species (684.5 eV) relative to the PVdF binder on the cathode surface film. This has also been observed in other cells containing GA[18,21] and SA[19,20] as electrolyte additives. The O 1s spectrum shows a large increase in oxygen-containing species in the 535.0–531.0 eV range. As the wt% of GA is increased in the cell the amount of oxygen-containing deposited species increases as well (as shown in the elemental concentration in Table III). According to the elemental concentration analysis, in the P 2p spectrum the peak at 134.5 eV arising from Li$_X$PO$_Y$F$_Z$ grows as the wt% of the GA additive is increased in the cell. This has been previously observed for cells containing GA[18,21] and SA[19,20] as electrolyte additives. Again, since the F 1s spectrum of Li$_X$PO$_Y$F$_Z$ overlaps the PVdF binder peak at 687.0 eV it is hard to see this species increase in that binding energy region.

It is easy to discern a drastic intensity decrease in the O 1s LiNi$_{0.5}$Mn$_{0.3}$Co$_{0.2}$O$_2$ metal-O bond at 529.6 eV with higher amounts of GA in the cell. This can be attributed to the formation of a more compact film on the surface of the cathode thus diminishing the binding energies coming directly from the cathode material.[24] This is corroborated by the C 1s data. Altogether, the increase in oxygen-containing surface species is attributable to an organic film composed of GA decomposition products, as opposed to phosphates or other inorganic species containing oxygen.

As noted previously, the observed C 1s peaks at 289.0 and 287.5 eV should arise from O-C=O and C=O containing species. Importantly, these moieties are inherently present in the GA structure and should be present in the decomposition species of GA. Additionally, the increase in peaks in the O1s spectrum indicate a substantial increase in oxygen-containing species on the cathode surface when compared to the baseline electrolyte. Thus, we can hypothesize that the additional peaks and increase in peaks in the O 1s and C 1s spectra for the GA containing cells correspond to the decomposition species of GA.

It is interesting to note that although less LiF was observed on the surface of the GA containing cells a higher impedance was observed for these cells. Looking at the XPS data it is clear that a more compact surface film most likely composed of organic species from GA decomposition is formed on the surface of the GA containing cells.
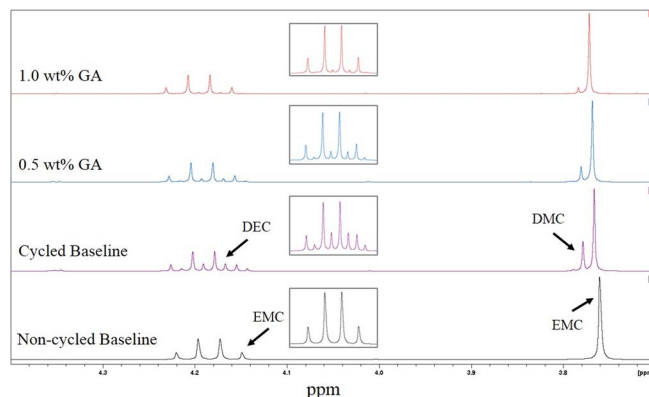
Figure 7. ^{1}H NMR analysis of cycled electrolyte solutions. Insets show the zoomed region between 4.25–4.11 ppm.

This data suggests that while the film formed on the cathode in the GA containing cells is more resistive than the baseline film, it is playing a beneficial role in the cycling performance of the cell.

Electrolyte decomposition species.—To get a better idea of the electrolyte solution of the cells post-cycling, solution state ^{1}H NMR was employed. After cycling the cells were opened in an Argon glove box and the internal components (spring, spacers, separator, electrodes) soaked in CDCl$_3$ for 30 seconds and then analyzed. The ^{1}H NMR spectra are shown in Figure 7. In non-cycled baseline electrolyte (1.2 M LiPF$_6$ in EC:EMC, 3:7 w/w) there are two peaks between 3.7–4.4 ppm: a quartet at 4.19 ppm and a singlet at 3.75 ppm both corresponding to the methylene and methoxy protons of EMC, respectively. After cycling with no additive a new quartet at 4.18 ppm and a new singlet at 3.78 ppm appear corresponding to a new observable species in solution. Looking at fresh solutions of DEC (4.18 ppm, methylene protons) and DMC (3.78 ppm, methyl protons) we can clearly see that the resonances of the newly observed peaks in the cycled baseline electrolyte correspond to these carbonate species. The occurrence of DEC and DMC in the cycled baseline electrolyte indicate that transesterifcation of EMC species is occurring during cycling. Interestingly, analysis of the electrolyte cycled with GA as an additive showed that with increasing amounts of GA the transesterification products of EMC can be partially suppressed. At least two hypotheses for this suppressed behavior can be reasoned: 1) GA prevents the transesterification products in the bulk solution, and or 2) GA prevents the transesterification products on the surface of the electrode. Reduction products of EMC (mainly lithium alkoxides) formed upon initial charging of the cell may then react with EMC in the bulk electrolyte in a nucleophilic fashion to generate the transesterification products. Alternatively, recent work done by Zhang et al. 2016 also noticed that upon cycling in Li/NMC half cells 1.2 M LiPF$_6$ in EC:EMC (3:7 w/w) showed that the DEC and DMC transesterication products of EMC could be inhibited using a fluorinated-phosphite electrolyte additive.[28] They hypothesized that additive decomposition products formed on the cathode surface as thin films blocked any transition metal catalyzed transesterification of the electrolyte.

Conclusions

The electrochemical performance of graphite/LiNi$_{0.5}$Mn$_{0.3}$Co$_{0.2}$O$_2$ full cells cycled between 3.0–4.4 V without and with GA as an additive in baseline electrolyte was examined. Using LSV we observed that the anodic stability of GA was less than the baseline electrolyte and therefore should preferentially oxidize compared to the electrolyte constituent parts. Additionally, the GA was shown to passivate the graphite electrode and suppress electrolyte reduction using Li/graphite half cells. The cycling performance of the cells containing GA as an additive in 1.0 and 0.5 wt% showed higher capacity retentions

and Coulombic efficiencies after 120 cycles when compared to the baseline electrolyte without GA. Differences in full cell impedance indicate that cells containing 1.0 and 0.5 wt% GA had higher overall impedances than the baseline cell. However, the ΔR_{SEI} and ΔR_{CT} between post-formation and post-cycling measurements was lowest in the 1.0 and 0.5 wt% GA cells suggesting the initial surface films formed during the formation cycles play a large role in determining the overall cell impedance. XPS of the cycled cathode surfaces showed a significant increase in oxygen-containing species and carbon containing species for the cells cycled with GA compared to the baseline electrolyte. More so, the cycled cathode electrodes indicated that cells containing GA as an electrolyte additive showed suppressed LiF formation and increased $Li_xPO_yF_z$ species formation. Additionally, NMR of the cycled electrolyte indicates a reduction in EMC transesterification products in GA cells suggesting a potential "blocking" of any transition metal catalyzed transesterification sites on the cathode surface. Additional studies investigating the passivation of the graphite electrode by GA are currently underway and should increase our knowledge of GA as an electrolyte additive. Overall, GA showed great promise as an electrolyte additive and the beneficial cycling performance of cells containing GA should arise from the more compact and protective film formed on the cathode surface.

Acknowledgments

References

1. B. Xu, D. Qian, Z. Y. Wang, and Y. S. Meng, "Recent progress in cathode materials research for advanced lithium ion batteries," *Mater. Sci. Eng. R*, **73**, 51, (2012).
2. S. B. Chikkannanavar, D. M. Bernardi, and L. Lingyun, "A review of blended cathode materials for use in Li-ion batteries," *J. Power Sources*, **248**, 91, (2014).
3. S.-M. Bak, E. Hu, Y. Zhou, X. Yu, D. Senanayake, S.-J. Cho, K.-B. Kim, K. Y. Chung, X.-Q. Yang, and K.-W. Nam, "Structural Changes and Thermal Stability of Charged LiNixMnyCozO₂ Cathode Materials Studied by Combined In Situ Time-Resolved XRD and Mass Spectroscopy," *ACS Appl. Mater. Interfaces*, **6**, 22594, (2014).
4. Y. K. Sun, S. T. Myung, B. C. Park, J. Prakash, I. Belharouak, and K. Amine, "High-energy cathode material for long-life and safe lithium batteries," *Nat. Mater.*, **8**, 320, (2009).
5. I. H. Son, J. H. Park, S. Kwon, J. Mun, and J. W. Choi, "Self-Terminated Artificial SEI Layer for Nickel-Rich Layered Cathode," *Chem. Mat.*, **27**, 7370, (2015).
6. Y. Zhu, Y. Li, M. Bettge, and D. P. Abraham, "Electrolyte additive combinations that enhance performance of high-capacity $Li_{1.2}Ni_{0.15}Mn_{0.55}Co_{0.1}O_2$–graphite cells," *Electrochim. Acta*, **110**, 191, (2013).
7. J. Li, L. Xing, R. Zhang, M. Chen, Z. Wang, M. Xu, and W. Li, "Tris(trimethylsilyl)borate as an Electrolyte Additive for Improving Interfacial Stability of High Voltage Layered Lithium-rich Oxide Cathode/carbonate-based Electrolyte," *J. Power Sources*, **285**, 360, (2015).
8. M. He, L. Hu, Z. Xue, C. C. Su, P. Redfern, L. A. Curtiss, B. Polzin, A. von Cresce, K. Xu, and Z. Zhang, "Fluorinated Electrolytes for 5-V Li-Ion Chemistry: Probing Voltage Stability of Electrolytes with Electrochemical Floating Test," *J. Electrochem. Soc.*, **162**, A1725, (2015).
9. S. Xu, R. M. Jacobs, H. M. Nguyen, S. Hao, M. Mahanthappa, C. Wolverton, and D. Morgan, "Lithium transport through lithium-ion battery cathode coatings," *J. Mater. Chem. A*, **17248–17272**, 3 (2015).
10. J. Zhang, Q. Lu, J. Fang, J. Wang, J. Yang, and Y. NuLi, "Polyimide encapsulated lithium-rich cathode material for high voltage lithium-ion battery," *ACS Appl. Mater. Interfaces*, **6**, 17965 (2014).
11. L. Hu, Z. Xue, K. Amine, and Z. Zhang, "Fluorinated Electrolytes for 5-V Li-Ion Chemistry: Synthesis and Evaluation of an Additive for High-Voltage LiNi0.5Mn1.5O4/Graphite Cell," *J. Electrochem. Soc.*, **161**, A1777 (2014).
12. Z. Zhang, L. Hu, H. Wu, W. Weng, M. Koh, P. C. Redfern, L. A. Curtiss, and K. Amine, "Fluorinated electrolytes for 5 V lithium-ion battery chemistry," *Energy Environ. Sci.*, **6**, 1806 (2013).
13. Y. Zhu, M. Bettge, and D. P. Abraham, "Positive Electrode Passivation by LiDFOB Electrolyte Additive in High-Capacity Lithium-Ion Cells," *J. Electrochem. Soc.*, **159**, A2109 (2012).
14. A. Nurpeissova, D.-I. Park, S.-S. Kim, and Y.-K. Sun, "Epicyanohydrin as an Interface Stabilizer Agent for Cathodes of Li-Ion Batteries," *J. Electrochem. Soc.*, **163**, A171 (2016).
15. X. Liao, Q. Huang, S. Mai, X. Wang, M. Xu, L. Xing, Y. Liao, and W. Li, "Self-discharge suppression of 4.9 V LiNi0.5Mn1.5O4 cathode by using tris(trimethylsilyl)borate as an electrolyte additive," *J. Power Sources*, **272**, 501 (2014).
16. Y.-M. Song, J.-G. Han, S. Park, K. T. Lee, and N.-S. Choi, "A multifunctional phosphite-containing electrolyte for 5 V-class LiNi0.5Mn1.5O4 cathodes with superior electrochemical performance," *J. Mater. Chem. A*, **2**, 9506 (2014).
17. G. Yan, X. Li, Z. Wang, H. Guo, and C. Wang, "Tris(trimethylsilyl)phosphate: A film-forming additive for high voltage cathode material in lithium-ion batteries," *J. Power Sources*, **248**, 1306 (2014).
18. Z. Wang, N. Dupré, L. Lajaunie, P. Moreau, J.-F. Martin, L. Boutafa, S. Patoux, and D. Guyomard, "Effect of glutaric anhydride additive on the LiNi 0.4 Mn 1.6 O4 electrode/electrolyte interface evolution: A MAS NMR and TEM/EELS study," *J. Power Sources*, **215**, 170 (2102).
19. V. Tarnopolskiy, J. Kalhoff, M. Nádherná, D. Bresser, L. Picard, F. Fabre, M. Rey, and S. Passerini, "Beneficial influence of succinic anhydride as electrolyte additive on the self-discharge of 5 V LiNi0.4Mn1.6O4 cathodes," *J. Power Sources*, **236**, 39 (2013).
20. R. Luo, D. Xu, X. Zeng, X. Li, J. Zeng, and S. Liao, "Enhancing the cycling stability of a carbonate-based electrolyte for high-voltage lithium batteries by adding succinic anhydride," *Ionics*, **21**, 2535 (2015).
21. H. Bouayad, Z. Wang, N. Dupré, R. Dedryvère, D. Foix, S. Franger, J.-F. Martin, L. Boutafa, S. Patoux, D. Gonbeau, and D. Guyomard, "Improvement of Electrode/Electrolyte Interfaces in High-Voltage Spinel Lithium-Ion Batteries by Using Glutaric Anhydride as Electrolyte Additive," *J. Phys. Chem. C*, **118**, 4634 (2014).
22. H. Lee, S. Choi, C. Choi, H.-J. Kim, Y. Choi, S. Yoon, and J.-J. Cho, "SEI layer-forming additives for LiNi0.5Mn1.5O4/graphite 5 V Li-ion batteries," *Electrochem. Comm.*, **9**, 801 (2007).
23. S. S. Zhang, K. Xu, and T. R. Jow, *EIS study on the formation of solid electrolyte interface in Li-ion battery*, **51**, 1636 (2006).
24. Z. Wang, L. Xing, J. Li, M. Xu, and W. Li, "Triethylborate as an electrolyte additive for high voltage layered lithium nickel cobalt manganese oxide cathode of lithium ion battery," *J. Power Sources*, **307**, 587 (2016).
25. Y. Kusachi, Z. Zhang, J. Dong, and K. Amine, "Electrode Surface Film Formation in Tris(ethylene glycol)-Substituted Trimethylsilane Lithium Bis(oxalate)borate Electrolyte," *J. Phys. Chem. C*, **115**, 24013 (2011).
26. L. Yang, B. Ravdel, and B. L. Lucht, "Electrolyte Reactions with the Surface of High Voltage LiNi0.5Mn1.5O4 Cathodes for Lithium-Ion Batteries," *Electrochem. Solid-State Lett.*, **13**, A95 (2010).
27. R. Dedryvère, S. Laruelle, S. Grugeon, L. Gireaud, J.-M. Tarascon, and D. Gonbeau, "XPS Identification of the Organic and Inorganic Components of the Electrode/Electrolyte Interface Formed on a Metallic Cathode," *J. Electrochem. Soc.*, **152**, A689 (2005).
28. M. He, C. Su, C. Peebles, Z. Feng, J. G. Connel, C. Liao, Y. Wang, I. A. Shkrob, and Z. Zhang, "Mechanistic Insight in the Function of Phosphite Additives for Protection of LiNi0.5Co0.2Mn0.3O2 Cathode in High Voltage Li-ion Cells," *ACS Appl. Mater. Interfaces*, **8**, 11450 (2016).